Aerotecnica Missili & Spazio, *The Journal of Aerospace Science, Technology and Systems*

Numerical study of 3D gaseous detonations in a square channel

S. Taileb, M. Reynaud, A. Chinnayya, F. Virot, P. Bauer[a]

[a]Institut Pprime, UPR 3346 CNRS-ENSMA-University of Poitiers,
BP 40109, 86961 Futuruscope Cedex, France

Abstract

The multidimensional structure of mildly unstable detonations are examined by numerical computations. These phenomenon have grown in interest since the development of propulsion devices such as pulsed and rotating detonation engines. Rectangular, diagonal and spinning modes are observed in a near-limit propagation detonation. High-order numerical integration of the reactive Euler equations have been performed to analyze the averaged structure, the shock dynamics of a single-cell detonation propagating in a square channel. Computations show a good agreement with the experimental cellular structure, showing the relevance of the slapping waves in the rectangular modes. The hydrodynamic thickness as well as the pdf shock dynamics are similar in the 2D and 3D cases, but the mean quantities vary on a quantitative basis. Moreover, the presence of strong forward jets is attested, which comes from simultaneous triple point line collisions with the walls.

1. Introduction

The gaseous detonation is a highly energetic phenomenon with fast reaction rates. An abrupt increase in the thermodynamic state, caused by a compression shock of the reactive medium leads to the chemical reaction initiation. Hence, the reactants are converted into products and expand downstream, self-sustaining the detonation front. These phenomena are involved in many application areas, such as propulsion, oil manufacturing, military devices, ballistics and industrial safety.

Detonations are naturally organized through a three-dimensional and transient structure. The latter is mainly formed of incident shocks and Mach stems, separated by triple point lines propagating onto the front surface. There are transverse waves at these junctions, which develop downstream of the detonation front and which propagate back and forth perpendicularly to the propagation direction. The trajectories of the triple point lines form the cellular structure of the detonation, of which height is closely related to the induction zone length. The generated flow downstream of the front is highly turbulent and the generated vortexes interact with the transverse shocks. Most of numerical studies have limited the investigation of this complex behavior to two-dimensional configurations. Because of limited diagnostics, the three-dimensional structure of the detonation and these interactions cannot be experimentally completely resolved in detail. Recently, performing 3D numerical simulations is becoming much more affordable with the increase of the computational capabilities. Thus, to some extent, it can offer a more accurate insight and a better understanding of the detonation dynamics.
Three dimensional numerical simulations were first performed by Williams et al. [1]. The computation were focused towards the detonation propagation in a square-channel and used a single-step global reaction modeling. The front structure was observed to be divided into rectangular areas delimited by the triple point lines. The comparison with two-dimensional computations revealed the presence of a slapping wave and a more intricate vorticity field in the three-dimensional case. Experimental studies were carried out by Hanana et al. [2] in order to confirm these numerical observations. They identified the rectangular mode of propagation and discovered the diagonal mode. This classification is the result of the triple point line trajectories onto the front surface. From the soot plate records, the motion of the triple point lines was found to be perpendicular to the walls in the rectangular mode, whereas in the case of diagonal mode, these lines move along the diagonal of the square section. Tsuboi et al. [3] performed numerical simulations with a detailed kinetic reaction mechanism and confirmed the earlier observations. Furthermore, they found out that the rectangular mode can be separated into two distinct behaviors: on-phase and out-of-phase. The simulations of Deiterding et al. [4] showed that the cell size differs between the different three dimensional modes, even though their geometri-

cal evolution exhibits many similarities. Eto et al. [5] also performed simulations for a hydrogen/air mixture in a rectangular tube using a detailed chemical model. They focused on the diagonal mode and demonstrated that the triple point line collisions generate a strong explosion located in the center and in the corners of the channel. These explosions generate pockets of unburnt gases, which are convected downstream of the front. Deledicque and Papalexandris [6] studied the geometrical similarities between the different modes. In the case of detonations where the cell size of the size of the channel, initial perturbations play a major role in the formation of these modes. The rectangular out-of-phase mode can be generated by a sinusoidal perturbation on the ZND initial profile. The diagonal mode was generated by a constant perturbation along the diagonal direction. Simulations in a narrower duct showed that this mode is unstable and evolves naturally into a spinning mode [7, 8]. Tsuboi et al. [9] computed numerous simulations of the spinning mode in circular and square tubes. Wang et al. [10] studied the effect of the influence of the duct size on the detonation modes. They show that as the duct size decreases, there is a threshold size below which the rectangular and diagonal modes break down and evolve into a spinning mode. Huang et al. [11] showed that the transverse wave dynamics and periodic pressure oscillations of the front are responsible of the transformations of the detonation structure from the rectangular/diagonal to the spinning mode.

This paper addresses the dynamics of the 3D detonation in a narrow square tube. Based on the previous experimental work from the literature, the results of the simulation are compared and discussed. The average profiles are used to shed light on the main differences that exist from the 1D, 2D and 3D simulations. The governing equations are presented in section 2. The section 3 describes the numerical solver employed and presents the physical configuration. The section 4 presents the numerical results for the instantaneous flow field and comparison with the experiments. The averaged profiles are presented in section 5. Finally, the paper is concluded with section 6.

2. Governing equations

The 3D reactive Euler equations are used for an ideal gas:

$$\frac{\partial U}{\partial t}+\frac{\partial F(U)}{\partial x}+\frac{\partial G(U)}{\partial y}+\frac{\partial H(U)}{\partial z}=\mathcal{S}(U) \quad (1)$$

where U, F, and G are the conserved variables vector, the x and y direction convective fluxes and the chemical source term vector, respectively. They read

$$U=\begin{bmatrix}\rho\\ \rho u\\ \rho v\\ \rho w\\ \rho E\\ \rho Y\end{bmatrix}, F=\begin{bmatrix}\rho u\\ \rho u^2+p\\ \rho uv\\ \rho uw\\ (\rho E+p)u\\ \rho Yu\end{bmatrix}, G=\begin{bmatrix}\rho v\\ \rho uv\\ \rho v^2+p\\ \rho uw\\ (\rho E+p)v\\ \rho Yv\end{bmatrix},$$

$$H=\begin{bmatrix}\rho w\\ \rho uw\\ \rho vw\\ \rho w^2+p\\ (\rho E+p)w\\ \rho Yw\end{bmatrix}, \mathcal{S}=\begin{bmatrix}0\\ 0\\ 0\\ 0\\ 0\\ \rho Y\dot{\omega}\end{bmatrix}$$

where u, v and w are the velocity components. ρ, p, E and Y are the density, the pressure, the total energy and the reaction advancement. The total energy, is expressed as

$$E=\frac{P}{(\gamma-1)\rho}+\frac{1}{2}(u^2+v^2+w^2)+Yq \quad (2)$$

where q is the heat release and γ is the specific heat ratio. The reaction mechanism is a one-step irreversible reaction, which turns the reactants into products $R\rightarrow P$. The chemical source term is assumed to follow the standard Arrhenius law,

$$\dot{\omega}=k(1-Y)\exp\left(-E_a/RT\right) \quad (3)$$

k, E_a and R are the constant rate coefficient, the activation energy and the gas constant, respectively. In order to the reaction rate to remain finite, a threshold is fixed for a mass fraction at 10^{-3}. To prevent the reaction to occur upstream of the leading shock, a pressure threshold was input as well.

The stability of premixed mixture, i.e. the regularity of the cellular structure is closely linked to the value of the activation energy. In order to control this parameter, several values of the reduced activation energy were used. The pre-exponential factor is adjusted for each value of the reduced activation energy value E_a/RT_0 in order to maintain the half-reaction length $l_{1/2}$ constant which also ensures that the cell size λ remains roughly constant [12]. The half-reaction length $l_{1/2}$ is defined as the distance between the incident shock and the point where $Y=\frac{1}{2}$ for the ideal ZND model.

3. Numerical methods

3.1. Numerical solver

The Euler equations are solved using a finite-difference method. The hydrodynamics is solved by a dimensional splitting and is coupled to chemistry by an operator splitting. In order to reduce dissipation and for a better accuracy, a high-order numerical scheme is implemented [13-14]. A ninth-order order Monotonicity Preserving interpolation is used to reconstruct the characteristics variables on the cell boundaries [13]. A HLLC Riemann solver is used to calculate the time-averaged fluxes of all conserved quantities at the cell

interfaces [14]. A third-order explicit TVD Runge-Kutta method is employed for the temporal resolution. A parallel computing strategy is implemented using a message passing interface system (MPI). A recycling process of the computational domain is used in order to reduce computational costs [12, 15]. The computations were performed on 400 processors, with a cost of about 45 000 CPU scalar hours per case.

3.2. Problem statement

The thermodynamic parameters are chosen to represent a stoichiometric $H_2 - O_2$ mixture at atmospheric conditions ($P_0 = 1$ atm, $T_0 = 295$ K). The ratio of specific heat and heat release are $\gamma = 1.333$ and $q = 4.867$ MJ/kg (i.e. $q/rT_0 = 23.81$), respectively. The CJ and von Neumann parameters are given in Table 3.2. These parameters have been calibrated in order to get the correct detonation velocity [16]. The other CJ parameters are obtained through classical relations.

D_{CJ}(m/s)	P_{CJ}(bar)	T_{CJ}	P_{vN}(bar)	T_{vN}(K)
2845	17.5	3007	34	1707

Table 1
Chapman-Jouguet (CJ) and von Neumann (vN) parameters

The computational domain is that of a rectangular channel. Outflow conditions are used for the upstream and downstream sections of the channel. The other boundary conditions are solid walls and slip conditions. The Figure 1 depicts the initial conditions. The domain is filled with fresh mixture, with some block areas set to the vN state, which correspond to an energy deposition.

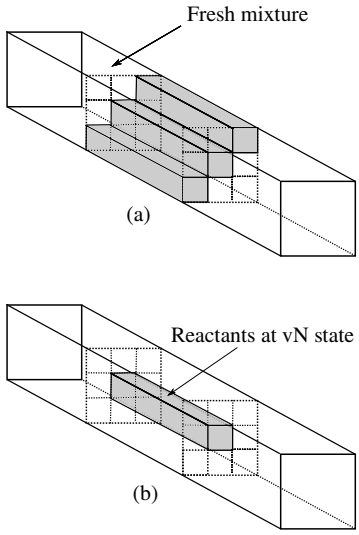

Figure 1. Schematic presentation of the initial conditions giving: diagonal (a) and rectangular (b) mode

4. Results and discussions

4.1. Shock front dynamics

The Figure 2 shows the evolution of the normalized front velocity as a function of the traveled distance, for the 1D, 2D and 3D simulations. They oscillate between 0.7 and 1.7. The average of the computational speed is 2856 m/s, which is 1% less than D_{CJ}. In the 1D case, the instability manifests itself as a longitudinal pulsation in the direction of the propagation. Indeed, small variations in the shock front temperature cause large fluctuations in the reaction rate. The detonation propagation resembles to a series of failures and re-initiations. Starting a cycle at the initiating phase, the normalized shock velocity jumps to 1.6. Then the shock decays rapidly to a value of order of the steady CJ value and remains at that value for a certain period. Then it fails abruptly and drops to a value about 0.7. At the end of this low-velocity phase, the detonation re-accelerates rapidly to an over-driven state for the next cycle. More information about this behaviour is given in Lee's book [17].

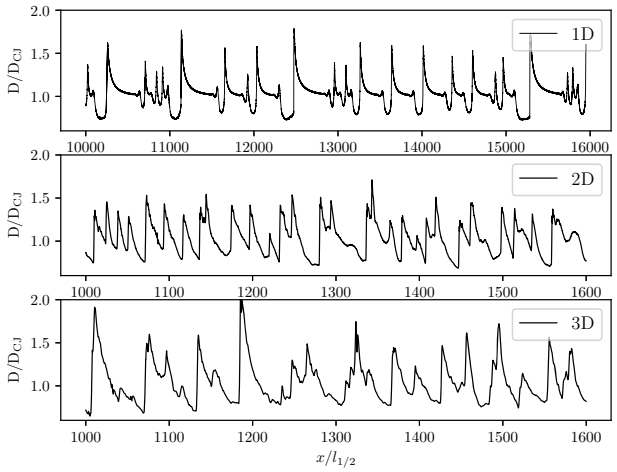

Figure 2. Instantaneous velocity of the shock front of the detonation, normalized by the CJ velocity D_{CJ} as a function of the distance, normalized by the half reaction length $l_{1/2}$ for the 1D, 2D and 3D cases.

The 2D and 3D profiles show a different trend. The detonation wave is composed of Mach stems and incident shocks linked to the transverse waves by the triple points. The spike is caused by the passage of the triple point along the line from which the front position is recorded, which is near the wall in the 2D case and near the corner in the 3D case. The front velocity decreases as the Mach stem becomes weaker in the cell and evolves into an incident shock. The low velocity is reached when the incident shock is much weaker than the averaged value, which can create a local decoupling of the shock with the reaction zone [18]. The frequency of these oscillations are similar in 2D and 3D simulations unlike the 1D from which the detonation pulsates at a much lower frequency.

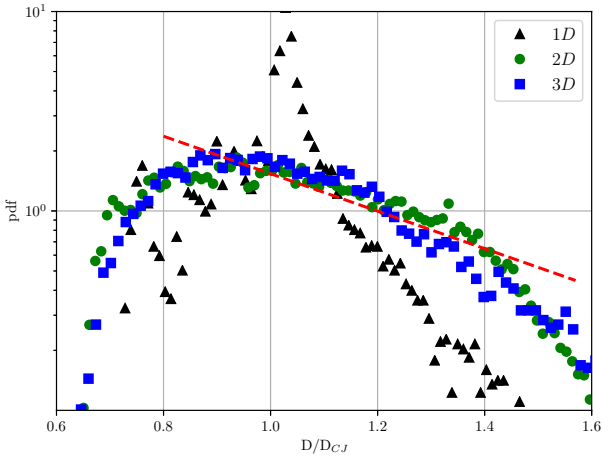

Figure 3. Probability density function of the leading shock velocity times series for the 1D, 2D and 3D cases. The red dashed line represents a power-law dependence with exponent -3.

The distribution of shock velocities is presented in Figure 3. In the 1D case, the two peaks corresponds to the 1.0 and 0.7 D_{CJ}, which correspond to the two phases described previously. In the multidimensional case, the distributions are similar but differ significantly from the 1D case. Multidimensional effects, such as e.g. local curvature tend to spread the 1D main peak. The pdf for the diagonal and the rectangular modes in the 3D case are very similar and follow the power-law dependence with exponent -3 [19]. The maximum of the PDF is around 2 for the normalized detonation velocity of 0.9. Moreover, the shock spends more time decaying into the cell. The acceleration occurs rapidly with the triple point interactions and transverse wave collisions. As a result, the shock velocity stays longer under the CJ conditions.

4.2. Global features

Different features can be exhibited according to the different modes. Indeed, depending on the initial perturbation, a rectangular or a diagonal mode is formed, which can be easily recognized from the front shape.

The Figure 4 exhibits the detonation front (grey iso-surface) and the maximum pressure history in the flow, in the case of a diagonal mode. The imprint of the triple points provides the cellular structure. From the first snapshot (top left), one can distinguish the incident shock in the middle of the front delimited by triple point lines from the Mach stems which are formed in the corners. New cells are formed from the triple line collision on the walls. As the triple point lines move towards the center of the channel, the incident shock surface is reduced.

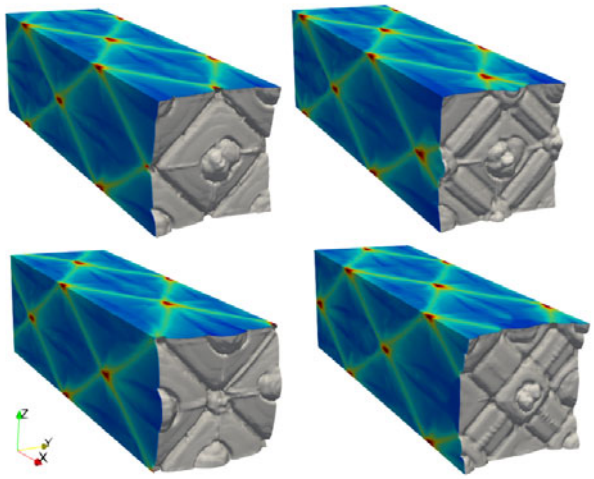

Figure 4. Detonation front structure in the diagonal mode, shown at different instants. The cell size λ is 2 mm.

In the rectangular mode (see Figure 5), the triple point lines are known to be perpendicular to the channel walls. When the triple point lines hit the walls, they imprint the slapping waves as well.
Moreover, jets are formed from the simultaneous collision of the orthogonal triple point lines on the wall. They are less strong and less frequent in the rectangular mode.

The evidence of the three-dimensional structure of the detonation front can be seen on the experimental soot-plates records. Figure 6 shows a comparison between the experimental soot-foil records from Hanana et al. [20] and the cellular structure derived from the numerical simulations, by taking the maximum value

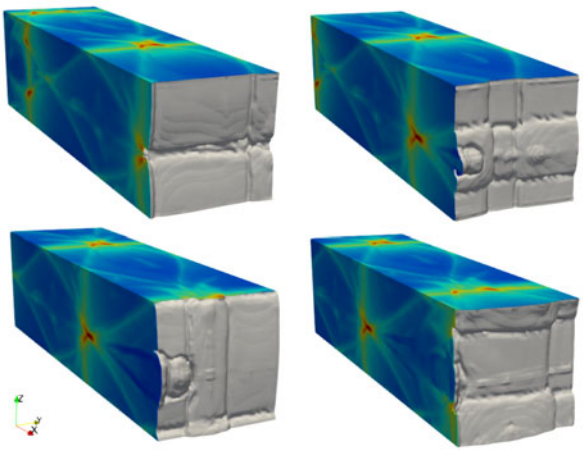

Figure 5. Rectangular front structure in the diagonal mode, shown in different positions in the cell. with the cell size width $\lambda = 1.3$ mm.

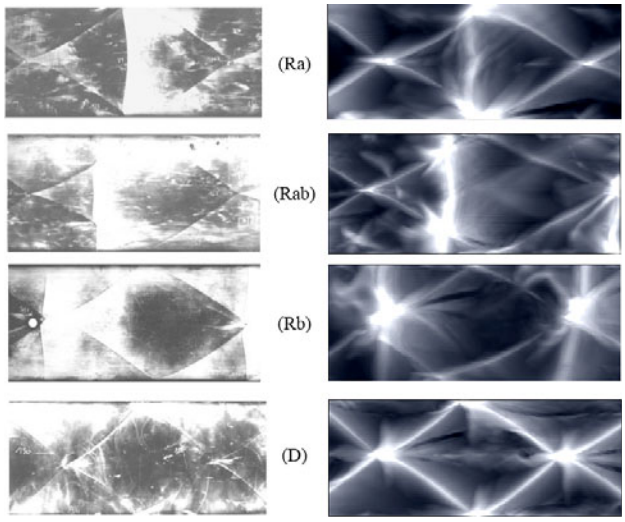

Figure 6. Comparison of the maximum pressure field for the cellular structure for $E_a/RT = 10$ (b) and typical experimental soot records from Hanana et al. [20] (a); cases (Ra), (Rab), (Rb) and (D) correspond to different types: in phase, partially out of phase, fully out of phase, and diagonal type, respectively

of the pressure field in each computational cell. Each picture shows a single detonation cell from one apex to the other. The first cases (Ra, Rab, Rb) of Figure 6 correspond to rectangular modes. The characteristic slapping wave is present and its position depends on the phase between the triple point lines. The mode is in phase for case (Ra), where the slapping wave impacts the center of the cell. The cases (Rab) and (Rb) correspond to out-of-phase modes of propagation, respectively.

5. Averaged structure

The averaged profiles are calculated during the simulation in the leading shock coordinates. The Favre average of any variable is ϕ is given by the relation $\widetilde{\phi} = \frac{\overline{\rho\phi}}{\bar{\rho}}$. The detection of the detonation front occurs via the pressure jump localization. Since the time averaging process takes place in the leading shock frame of reference, the averaged profiles are shifted during the computation in order to match with the instantaneous ones.

The following results correspond to a diagonal mode for the mildly unstable detonation $\mathrm{E_a/RT} = 38.23$, which correspond to kinetic parameters representative of the $2H2 + O2$ [12]. More details on the averaging procedure can be found in references [12, 19, 21].

The Figure 7 displays the evolution of the mean pressure as a function of the distance from the leading shock for the ZND stationary model, 1D, 2D and 3D simulations. The variation of the averaged local mach number $\widetilde{M} = \widetilde{u}/(\gamma\bar{p}/\bar{\rho})^{1/2}$ as a function of the distance from the front shock is displayed in Figure 8. The mean profiles differ significantly from the ZND profile. And mean quantities also differ on a quantitative ba-

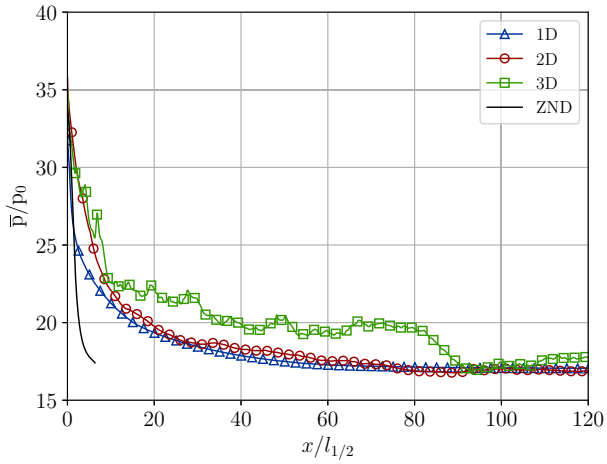

Figure 7. Normalized pressure profiles for the ZND, 1D, 2D and 3D (rectangular) with $E_a/RT = 38.23$

sis, as the number of dimensions increases. The mean pressure profiles are smoother than the instantaneous profiles. As compared to the ZND stationary profile, the sonic plane is clearly delayed. This is due to the presence of the fluctuations, induced by the longitudinal and transverse instabilities, which are responsible of the cellular structure. The hydrodynamic thickness, which is the mean distance between the leading shock

and the sonic plane increases slightly from the 1D case to the multidimensional cases. For the 1D case, the pressure and the Mach number relax smoothly to the sonic plane. In the 3D case, the non-monotonic Mach number profile is due to the presence of the slapping waves.

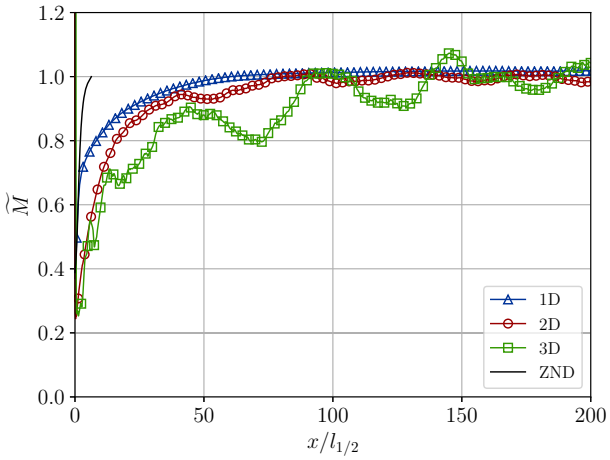

Figure 8. Mach number profiles for the mildly unstable case for the ZND, 1D, 2D and 3D (rectangular) detonation wave

6. Conclusions

Three-dimensional detonation simulations in narrow channel have been performed with the Euler reactive model and a high-order numerical scheme. Two different initial conditions lead to different detonation rectangular and diagonal modes. The detailed analysis of the structure of these modes have shown good agreement with the available experimental studies. The simulation correctly resolves the characteristic cellular structure, showing the importance of the slapping waves in the rectangular modes. Moreover, the numerical results demonstrate the relevance of multidimensional effects, even in mildly unstable mixtures such as stoichiometric $H_2 - O_2$, even if these effects on the hydrodynamic thickness is less pronounced. The hydrodynamic thickness and the pdf of the shock velocity are globally the same in 2D and 3D, but the mean quantities differ on a quantitative basis. Moreover, the presence of forward jets, of which formation come from the simultaneous triple point line collision with the walls can be noticed. They are much stronger than in the 2D case. Further investigations are necessary to quantify these influences more clearly. Indeed, the averaged quantities can be dependent on the detonation propagation mode and on the spatial location.

REFERENCES

1. D. N. Williams, L. Bauwens, E. S. Oran, Detailed structure and propagation of three-dimensional detonations, in: Symposium (International) on Combustion, Vol. 26, Elsevier, 1996, pp. 2991–2998.
2. M. Hanana, M. Lefebvre, Pressure profiles in detonation cells with rectangular and diagonal structures, Shock Waves 11 (2) (2001) 77–88.
3. N. Tsuboi, S. Katoh, A. K. Hayashi, Three-dimensional numerical simulation for hydrogen/air detonation: Rectangular and diagonal structures, Proceedings of the Combustion Institute 29 (2) (2002) 2783–2788.
4. R. Deiterding, Numerical structure analysis of regular hydrogen-oxygen detonations, in: WSSCI Fall 2003 Meeting, University of California, Los Angeles, 2003.
5. K. Eto, N. Tsuboi, A. K. Hayashi, Numerical study on three-dimensional cj detonation waves: detailed propagating mechanism and existence of OH radical, Proceedings of the Combustion Institute 30 (2) (2005) 1907–1913.
6. V. Deledicque, M. V. Papalexandris, Computational study of three-dimensional gaseous detonation structures, Combustion and flame 144 (4) (2006) 821–837.
7. H.-S. Dou, H. M. Tsai, B. C. Khoo, J. Qiu, Simulations of detonation wave propagation in rectangular ducts using a three-dimensional WENO scheme, Combustion and Flame 154 (4) (2008) 644–659.
8. H. S. Dou, B. C. Khoo, Effect of initial disturbance on the detonation front structure of a narrow duct, Shock Waves 20 (2) (2010) 163–173. doi:10.1007/s00193-009-0240-8.
9. N. Tsuboi, A. K. Hayashi, Numerical study on spinning detonations, Proceedings of the Combustion Institute 31 (2) (2007) 2389–2396.
10. C. Wang, C.-W. Shu, W. Han, J. Ning, High resolution WENO simulation of 3D detonation waves, Combustion and Flame 160 (2) (2013) 447–462.
11. Y. Huang, H. Ji, F. Lien, H. Tang, Numerical study of three-dimensional detonation structure transformations in a narrow square tube: from rectangular and diagonal modes into spinning modes, Shock Waves 24 (4) (2014) 375–392.
12. M. Reynaud, F. Virot, A. Chinnayya, A computational study of the interaction of gaseous detonations with a compressible layer, Physics of Fluids 29 (5) (2017) 056101.
13. A. Suresh, H. T. Huynh, Accurate monotonicity-preserving schemes with runge–kutta time stepping, Journal of Computational Physics 136 (1) (1997) 83–99.
14. E. F. Toro, M. Spruce, W. Speares, Restoration

of the contact surface in the HLL-riemann solver, Shock Waves 4 (1) (1994) 25–34.
15. A. Sow, Modélisation numérique des détonations gazeuses en milieu confiné, Ph.D. thesis, University of Rouen, France (2014).
16. O. Heuzé, P. Bauer, H. Presles, C. Brochet, Equations of state for detonation products and their incorporation into the quatuor code, in: 8th Symp.(Int.) on Detonation, 1986, pp. 762–769.
17. J. H. Lee, The detonation phenomenon, Cambridge University Press Cambridge, 2008.
18. J. M. Austin, The role of instability in gaseous detonation, Ph.D. thesis, California Institute of Technology (2003).
19. M. I. Radulescu, G. J. Sharpe, C. K. Law, J. H. S. Lee, The hydrodynamic structure of unstable cellular detonations, Journal of Fluid Mechanics 580 (2007) 31–81.
20. M. Hanana, M. H. Lefebvre, P. J. V. Tiggelen, Pressure profiles in detonation cells with rectangular and diagonal structures, Shock Waves 11 (2001) 77–88.
21. A. Sow, A. Chinnayya, A. Hadjadj, Mean structure of one-dimensional unstable detonations with friction, Journal of Fluid Mechanics 743 (2014) 503–533.